Sensing and Imaging (2024) 25:13
https://doi.org/10.1007/s11220-023-00456-z

RESEARCH

# Hybrid Optimization Enabled Segmentation with Deep Learning For Histopathological Images of Uterine Tissue

**Veena I. Patil[1,2] · Shobha R. Patil[3]**

Received: 6 April 2023 / Revised: 5 October 2023 / Accepted: 19 December 2023


## Abstract

The technique of modifying an image to make it better suited for a certain use than the original image is known as image enhancement. Digitalized picture enhancement systems provide numerous choices for improving image visual quality. Imaging modalities, observation settings, and other factors all have a substantial impact on the appropriate choosing of various methodologies. The Fractional Pelican Crow Search Algorithm improved SQA (FPCSO_ enhanced SQA) is a novel image enhancement technique for histopathology imaging of uterine tissue that is provided here. The database is initially generated, and the image is forwarded to the pre-processing phase. In order to reduce noise and enhance image quality, the median filter is employed in image pre-processing. Additionally, image enhancement is done utilizing the Pelican Crow Search Algorithm-trained Multiple Identities Representation Network. After the image enhancement, the tissue segmentation is performed using proposed segmentation quality assessment network, where parameter selection is based on Deep Convolutional Neural Network (DCNN). Here, DCNN is trained using proposed FPCSO algorithm. Accordingly, proposed FPCSO approach is newly integrated by the combination of Pelican Optimization Algorithm, Crow Search Optimization and Fractional calculus. Furthermore, FPCSO-enhanced SQA-reached best consequences with maximal Peak signal-to-noise ratio (PSNR) of 49.574 dB, minimum Mean Square Error of 0.975, and minimum degree of distortion of 0.061 dB, correspondingly.

**Keywords** **M**edian filter · Deep learning · Multiple identities representation network · Pelican crow search algorithm · Uterine tissue

Extended author information available on the last page of the article

Published online: 17 February 2024

## 1 Introduction

The medical industry is one such field where, at the moment, attentive information utilisation can aid in the development of people's health and in tasks namely diagnostics. Images-based computer applications include X-rays, ultrasonic imaging (sonography), magnetic resonance imaging (MRI), computed tomography (CT), and magnetic resonance imaging (MRI).In addition to these photos, histopathology images are another sort of medical image that is regarded as the gold standard for cancer detection [1]. Medical image valuation necessitates proficient and valuable representation of image contents in order to handle big, potentially complex collections. Meanwhile the past span, there has been a remarkable rise in processing capacity and advancement in computer-assisted investigative techniques towards medical data. Medical image analysis can supplement radiologists' judgement. Histopathological specimen images can now be scanned and saved as a digital image. As a result, they are readily available in vast quantities to academics that use various image analysis algorithms and machine-learning approaches to investigate them [2]. Even though histopathological pictures contain significant information about cell shape and tissue architecture, they are employed in a variety of clinical applications [3, 4], including medical diagnosis [5], cancer malignancy grading, and therapy effectiveness prediction [6]. Yet, a Pathologist's manual assessment of histological pictures is time consuming and subjective. The goal of digital histopathology image analysis is to analyse histopathological pictures automatically, which can considerably enhance diagnostic repeatability and objectivity [5]. Segregating each nucleus in histological pictures, in particular, is a fundamental and vital task [7].

Worldwide, 529,000 new instances of offensive cervical cancer were described in 2008. Although developing world bears the brunt of the burden of cervical cancer prevalence, invasive cervical cancer is still detected in the United States every year. Cervical cancer and its precursor lesions can be found with a Pap test, colposcopy to examine cervix physically, and a specialist's microscopic review of histology slides when a biopsy sample of cervix tissue is provided. A qualified pathologist's microscopic examination of histology slides has been utilised as a diagnostic standard. Cervical Intraepithelial Neoplasia (CIN) is a pre-malignant condition for cervical cancer that is diagnosed by visual evaluation of histology slides as part of the pathologist diagnostic procedure [8]. Most cases of uterine cancer are endometrial carcinoma. It's usually referred to as uterine cancer because of the endometrium's link to the uterus. Gynecologic cancers affecting the uterus, ovaries, cervix, vagina, vulva, and fallopian tubes are all included in the most prevalent type of gynecologic cancer, known as endometrial cancer. While pregnant the endometrium thickens to support the fetes and sheds throughout the menstrual cycle. Uterine cancer must be diagnosed, graded, and classified using a pelvic examination, endometrial biopsy/fractional dilation, curettage, and microscopic inspection of biopsy materials..Visual interpretation of biopsies is time—incontrollable process, labour hard, and largely dependent on medical professional's knowledge and experience. If computer systems can perform such analysis, then diagnosis, grading, and classification of biopsies can be accomplished quickly using textural or architectural analysis [9].

In affluent countries and less developed nations, uterine carcinoma is the second most common gynaecologic malignancy. Although they only account for 10–15% of endometrial cancer, uterine serous and clear cell carcinoma account for up to 40% of cancer-related fatalities in uterine cancers. They are thought to be more destructive clinically than endometriosis carcinoma. Patients with non-endometriosis carcinoma had a much worse prognosis than patients with uterine endometriosis adenocarcinomas, even in stage I illness [10].Since computer-aided diagnosis (CADx), also recognised as computer-aided detection (CADe), can help doctors analyse and evaluate a large number of medical images, such as ultrasound images and X-rays, it has been used in the radiologic diagnostic test of some common cancers, such as breast cancer, lung cancer, and colon cancer, in clinical settings. In recent years, a few researchers have also created CADx-systems to process hysteroscopic [11], ultrasound [12], magnetic resonance, and histopathological images for early diagnosis of endometrial cancer. One of the most intriguing new developments in machine learning is deep learning, which has proven to be highly effective in a variety of practical uses. A variety of rare or specialised malignancies, such as skin cancer, congenital cataracts, bacterial and viral pneumonia, diabetic retinopathy, and congenital cataracts, have been detected using digital image-based techniques, demonstrating human expert-level performance in disease categorization. Hence, the combination of CADx with deep learning has the potential to significantly increase the efficacy of existing CADx systems for endometrial cancer using big data in medical image [13].

The main goal is to provide an effective method for FPCSO-enhanced SQA, which is a methodology for improving the appearance of histopathology pictures of uterine tissue. Using tissue images of uterine endometrium, a database of histopathological images of uterine tissue is built here and sent to pre-processing stage. The median filter [14] is used in the pre-processing step to reduce noise from input images, hence improving image quality. Following image enhancement, tissue segmentation is carried out using the suggested segmentation quality evaluation network, with parameters chosen using DCNN. Here, DCNN is qualified using FPCSO algorithm. Accordingly, developed FPCSO approach is newly integrated by combination of POA, CSA and FC.

The key influence of this work is explained below.

*Developed FPCSO_enhanced SQA for histopathological images of uterine tissue* An efficient method named FPCSO_enhanced SQA for histopathological images of uterine tissue. MIRNet is used to improve the images in this case, and it is trained using PCSO. Additionally, tissue segmentation is performed using the suggested segmentation quality evaluation network, with parameters chosen using the proposed FPCSO based on DCNN. Moreover, developed FPCSO is the combination of FC, CSA, and POA.

The following describes the paper's structure: Part 2 contains the remainder of this study, information on the sources of inspiration, evaluations of the literature, and challenges with uterine tissue. Section 3 shows the FPCSO_enhanced SQA block diagrams for histological imaging of uterine tissue. Part 4 presents investigational study, and Sect. 5 discusses conclusion.

## 2 Motivation

As a confirmation test for uterine cancer identification, pathologists' eye examination of histopathological uterine tissue samples is accepted. A manual segmentation is dependent on pathologists' involvement, and hence issue is substantial analysis. This led to the creation of a novel method for improving uterine tissue histopathology images. Some conventional works are assessed in light of this principle and are discussed more below.

### 2.1 Literature Review

Qu et al. [10] introduced an efficient method named multi-institutional pooled assessment for discovering the accountability of adjuvant therapy in handling endometrial cancer. Due to the lack of a centralized pathology examination offered in this technique for diagnosis confirmation, despite the significantly higher detection rate and individual chart evaluation, the method was nevertheless unsuccessful. Wright et al. [15] established sentinel lymph node (SLN) biopsy for endometrial cancer wherein cost of this method was condensed in long and short-term and false negative rate was reduced. A lesser number of women who underwent SLN biopsy were excluded from other examinations since it required longer-term follow-up and was not counted. Patil and Patil [9] presented Morphological operation and thresholding to distinguish nuclei cell in the histopathological imageries of uterine cancer. It provided a simpler way for clinical specialists to undertake evaluation work, but it did not separate touching nuclei. Jones et al. [16] created immunogenicity markers that showed to be able to proliferate for high-grade cancers and preferentially benefited from immune therapy, whereas metastatic tumors assessment did not indicate a difference.

Eman Hussein Alshdaifat et al. [17] designed a retrospective chart review to determine the histological pattern of endometrial samples in patients. It was proven to be very credible and precise, however it was unable to assess interrater dependability between diagnosticians. Sun et al. [13], developed Convolutional Neural Network and Attention (CNN + Attention) for diagnosing histological images of endometrial disorders. It provided the best diagnostic interpretability; however, it did not gather enough endometrial tissue samples to enrich the dataset. Guo et al. [8], established a cellular and atypical cell concentration feature based on vertical segmentation separations of epithelial area. It classified cervical intraepithelial neoplasia (CIN) grade with excellent grade labelling accuracy but did not use adaptive critic design. Solar and Gonzalez [18], developed a computational technique for assessing exfoliative cytology of the cervix, which lowered false negatives and false positives while failing to improve detection rate.

### 2.2 Challenges

Some of the significant challenges that the histopathological images for uterine tissue techniques have experienced are as follows:

- An efficient method named multi-institutional pooled assessment was developed in [10], for handling endometrial cancer. Here, the method achieved high detection rate. It was unsuccessful, since there was no centralized pathologic review.
- The SLN biopsy created in [15] for endometrial cancer was less expensive and took less time to conduct, however SLN biopsy coding was dependent on procedure count as well as charge code.
- Morphology operation and thresholding in [9] were established for nuclei recognition in histopathology pictures of uterine cancer, but it did not take into account nuclei features for cancer cell identification.
- In [16], immunogenicity markers failed to give clinically relevant conclusions from datasets that lacked patient demographics, tumor histology, and treatment information.
- Effectively choosing patients at risk for severe surgery and offering appurtenant behavior in the event that low risk individuals are over treated are two clinical challenges associated with endometrial cancer.

## 3 Proposed FPCSO_Enhanced SQA for Histopathological Images of Uterine Tissue

The main objective of image enhancement is to modify some features of the image to improve its suitability for a particular purpose and viewer. Identifying tumors in histological pictures is always thought to be a difficult task. FPCSO_enhanced SQA is a new technique for histopathology imaging of uterine tissue. Initially, a database is constructed and sent to the pre-processing step. A median filter is used in picture pre-processing to remove noise and develop image superiority. Subsequently, image enhancement is carried out using MIRNet, which has been tweaked by designed PCSO. Additionally, tissue segmentation is performed using the suggested segmentation quality evaluation network, with parameter selection based on DCNN, which is trained on the proposed FPCSO. Furthermore, FPCSO is incorporation of FC, POA and CSA. Pictorial view of established FPCSO_enhanced SQA for image enhancement is described in Fig. 1.

### 3.1 Database Creation

The database of histological images of uterine tissue is built from [19], and the database building process is as follows. First, open hankie photos of uterus endometrium from the specific link, which contains both normal and diseased tissues. The tissue

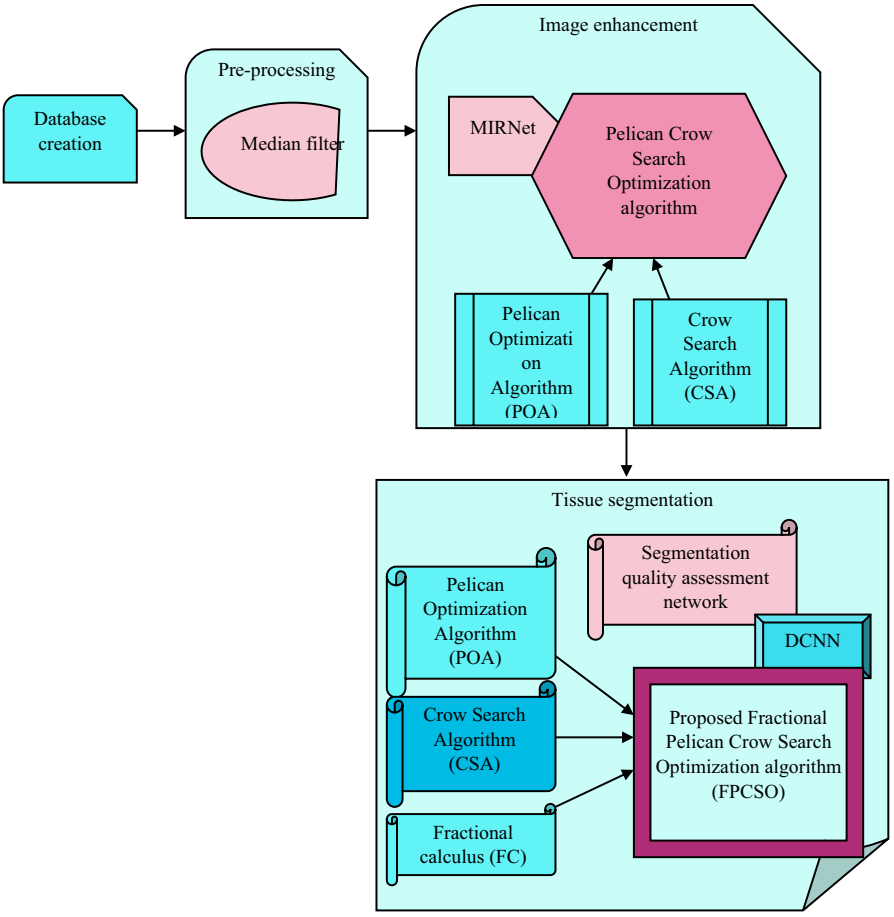


**Fig. 1** Block diagram of proposed FPCSO_enhanced SQA for histopathological uterine tissue segmentation

is then magnified in 20 different regions and cropped into 20 picture samples. As a result, for each uterus endometrial sample, 20 images are obtained, with 10 imageries being usual and 10 imageries being irregular. Eventually, same method is followed, yielding 400 photos, 200 of which are normal and 400 of which are aberrant. The constructed database can be depicted as,

$$\Upsilon = \left\{\Upsilon_1, \Upsilon_2, ..., \Upsilon_e, ..., \Upsilon_z\right\} \tag{1}$$

wherein, the overall images included in database $\Upsilon$ are detailed by $z$ while $e^{th}$ image is signified by $\Upsilon_e$.

### 3.2 Pre-processing Using Median Filter

The second stage of histopathological images of uterine tissue is pre-processing, and $\Upsilon_e$ is the image fed during this stage. The results of picture quality evaluation are particularly impacted by image pre-processing. The mathematical normalizing of a database, which is a common step in many feature description approaches, can be compared to the pre-processing of an image. Pre-processing is essential to improve image quality by removing obstacles caused by color discrepancies and by removing noise from an image. In this scenario, image pre-processing employs median filter. The median filter [14] examines pixel size in a certain region and removes the median from a domain as the newer value of the domain's center pixel. Rapid sorting is the foundation of a typical median filter method. There is some edge blurring when using a non-linear filtering technique. It keeps information at the borders of the image in addition to removing or greatly reducing random noise and pulse interference. One way to express the median filter is,

$$\mathbb{N}_x = \widehat{D}\,(k,l) \;= median\left\{t(a,b),\,(a,b) \in G_{kl}\right\} \tag{2}$$

wherein, noise is represented as $t\,(a,b)$, and yield pixel value of filtering result is signified as $\widehat{D}\,(k,l)$, which is arrangement median value while filtered image is denoted as $N_x$.

### 3.3 Image Enhancement Using FPCSO_Enhanced SQA

Pre-processed image $N_x$ is provided as an input for image enhancement method. Image enhancement [20] improves the overall appearance and ability of an image in order to pick spatial features. Image enhancement software often enhances human eyesight and raises the likelihood that automated image processing will be successful. Here, histopathology images of uterine tissue are improved using MIRNet. On the other side, PCSO, a mix of POA and CSA, trains MIRNet.

#### 3.3.1 Architecture of MIRNet

Multi-scale residual block (MRB), a crucial part of the network, is capable of performing image enhancement and image de-noising in MIRNet [21]. Below is a full explanation of each MIRNet component, and Fig. 2 depicts the MIRNet design.

For a specified image $J \in \hbar^{R\times H\times 3}$, the system primarily smears convolutional layer for removing low level features $T_0 \in \hbar^{R\times H\times Z}$. Formerly, feature maps $T_0$ permits to M count of recursive residual groups (RRG) that harvests deep features $T_1 \in \hbar^{R\times H\times Z}$. Afterwards, convolutional layer is practical to deep features $T_1$ and achieves residual image $U \in \hbar^{R\times H\times 3}$. Lastly, reinstated image is developed as $\widehat{J} = J + U$.

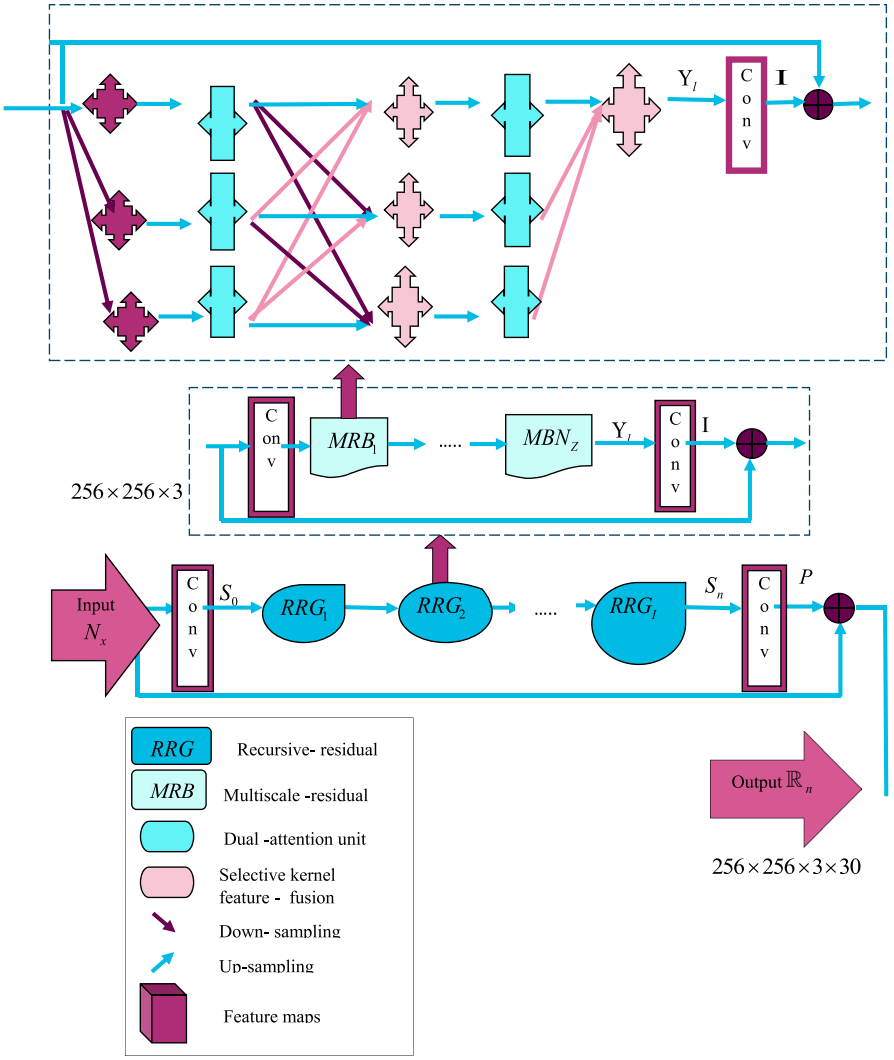


**Fig. 2** Architecture of MIRNet

**3.3.1.1 MRB** While handling high resolution depictions and obtaining rich background information from low resolutions, it is able to produce spatially accurate output. A number of completely connected, parallel streams make up the MRB. It enables the flow of information between parallel streams, allowing low resolution features to assist in the consolidation of high-resolution features and so on. Each MRB component is explained in the following.

Selective kernel feature fusion (SKFF)

Self-attention system is used by the MRB's SKFF, a non-linear approach, to merge features from various resolutions. Using two functions first, fuse, then select it implements dynamic modifications to receptive fields. These descriptors are used by select operators to calibrate feature maps from various streams prior to aggregation, whereas fuse operators produce global feature descriptors by combining data from several resolution streams. The two operators are quickly explained as follows:

*(i) Fuse* Three convolution streams running in parallel with varying information scales provide SKFF with an input. These multiscale characteristics are integrated using the element-wise sum that is depicted below.

$$\lambda = \lambda_1, \lambda_2, \lambda_3 \tag{3}$$

Hence, regardless of spatial scale, global average pooling (GAP) is useful of $\lambda \in \hbar^{r \times H \times Z}$ for calculating channel-wise figures $v \in \hbar^{J \times 1 \times Z}$. Subsequently, channel rationalizing complication layer is useful for producing compact feature representation $w \in \hbar^{J \times 1 \times h}$, where $h = \frac{Z}{8}$. Lastly, feature vector offers three feature signifiers denoted as $r_1, r_2,$ *and* $r_3$ and is enabled by three parallel channel upscaling convolution layers, each consuming dimension $1 \times 1 \times Z$.

*(ii) Select* In this phase, the select operator smears Softmax role to $r_1, r_2,$ *and* $r_3$ by elastic courtesy initiations $v_1, v_2$ *and* $v_3$, which is applied to adaptively the recalibrating multi-scale feature maps $\lambda_1, \lambda_2$ *and* $\lambda_3$. The total feature accumulation and recalibration procedure is well-defined by,

$$E = v_1 \lambda_1 + v_2 \lambda_2 + v_3 \lambda_3 \tag{4}$$

Dual attention unit (DAU)

It was created to excerpt features from convolutional watercourses. Less useful aspects are suppressed by DAU, and only highly informative features are allowed to continue operating. By using channel attention and spatial attention methods, the feature calibration is accomplished.

### 3.4 Channel Attention (CA)

By using techniques like excitation and squeeze, it takes advantage of a relationship between convolutional feature maps on different channels. Squeezing over the spatial sizes for a given feature map $\xi \in \hbar^{R \times H \times Z}$ results in feature descriptor $\eta \in \hbar^{1 \times 1 \times Z}$ when GAP is used to encode global context. In two convolutional layers, followed by sigmoid gating, an excitation operator forms $\widehat{\eta} = \hbar^{1 \times 1 \times Z}$ by passing by $\eta \in \hbar^{1 \times 1 \times Z}$.By rescaling $\xi$ with activations $\widehat{\eta}$, CA output is finally obtained.

### 3.5 Spatial Attention (SA)

It was created to take advantage of inter-spatial dependence of convolutional features. In order to calibrate incoming features $\xi$ SA aims to produce a spatial awareness map. The SA first performs GAP and max-pooling procedures on features $\xi$ beside channel dimensions, after which result is concatenated to create the feature map $\psi \in \hbar^{R\times H\times 2}$.In order to create a spatial attention map $\widehat{\psi} \in \hbar^{R\times H\times 1}$ that is used to rescale $\xi$, the map $\psi$ is subjected to convolution and the sigmoid function.

## 4 Residual Resizing Modules

Information flow during a learning process is facilitated by the use of the recursive residual design. For up- and down-sampling procedures, residual resizing techniques are developed to protect residual nature. The size of the feature maps is constant in MRB along convolution streams. Alternately, the input and output resolution index, indicated by the letters *u and i* affects the size of the feature map differently across streams.An input feature tensor is down sampled if $u < i$, but an up sampled feature map is produced if $u > i$. As a result, $\mathbb{R}_n$ stands for the enhanced image from MIRNet.

### 4.1 Tissue Segmentation Using SQA Network

The DCNN, which accumulates evidence from CNN, obtains the enhanced image $N_x$ as its input. A segmentation result's quality is to be evaluated by segmentation quality assessment [22]. Similar to how methods for evaluating the quality of pictures are separated into two categories, segmentation quality assessment techniques can be classified as non-blind and blind. The initial attempts to measure the segmentation outcomes using the ground truth in order to gauge how much the segmentation result and the ground truth resemble one another on a more perceptual level. In the second method, the segmentation quality is evaluated without the need of a ground truth and is determined only by recognizing the relevant quality cues from the segmentation results.

#### 4.1.1 Problem Formulation

In order to forecast a score $\alpha$ within the range of [0,1] that indicates quality of $C$, which can be signified by,

$$\alpha = CNN_{\alpha}(K, C) \tag{5}$$

Here, $CNN_{\alpha}$ indicates network of CNN, which is used to attain the estimation.

#### 4.1.2 Baseline

Two steps in the network are used for the baseline segmentation quality assessment: the feature extraction phase and the quality prediction phase.VGG-16 network is used as the first phase, and then three FC layers are applied. By normalizing the final FC layer with a sigmoid layer, the assessment score is achieved.

#### 4.1.3 DCNN Network

Convolutional, non-linear, fully connected, and pooling layers make comprise layers of a DCNN, a form of artificial neural network. Figure 2 displays the DCNN's architectural layout. DCNN [23] layers are described as follows:

**4.1.3.1 Convolutional Layer** This layer contains numerous filters that slide above it for particular input data. After that, a basic filter multiplication and a tractable input field are added to calculate the output layer. It can be modeled by,

$$(A_i^y)_{d,u} = (V_i^y) + \sum_{\iota=1}^{\kappa_1^{\iota-1}} \sum_{\vartheta=\kappa_1^y}^{\kappa_1^y} \sum_{\omega=\kappa_2^y}^{\kappa_2^y} (\mathbb{Z}_{i,\iota}^y)_{\omega,\vartheta} * (A_{\mu}^{y-1})_{d+\vartheta,\chi+\omega} \tag{6}$$

In this occurrence, the appearance $(A_i^y)_{d,u}$ signifies fixed feature chart or the output of $y$th convolutional layers that is decided as $(d, u)$. An input to $l$th convolutional layer is formed from an output of $(y-1)^{th}$ layer's previous layer. Convolutional layer masses are denoted as $(\mathbb{Z}_{i,\iota}^y)_{\omega,\vartheta}$, and weight of the $y$th convolutional layer is $V_i^y$. Rectified Linear Unit (Re$LU$) layer employs an element-wise stimulus purpose, and output from $l^{th}$Re$LU$ layer is instigation function of the $(\sigma-1)^{th}$ preceding layer and is intended as follows:

$$(A_i^y) = A_{\phi}(A_i^{y-1}) \tag{7}$$

$$\text{Re}LU = \begin{cases} 0, & if\ Q_f < 0 \\ Q_f & if\ Q_f \geq 0 \end{cases} \tag{8}$$

**4.1.3.2 Pooling Layer** Although being non-parametric, this layer roughly decreases the inputs' dimension and serves an eternal purpose.

**4.1.3.3 Fully Convoluted Layer** The pooling layer then sends data to the fully linked layer. Understanding the non-linear aggregation of features used by these layers as a classifier is necessary. The sentence below creates it.

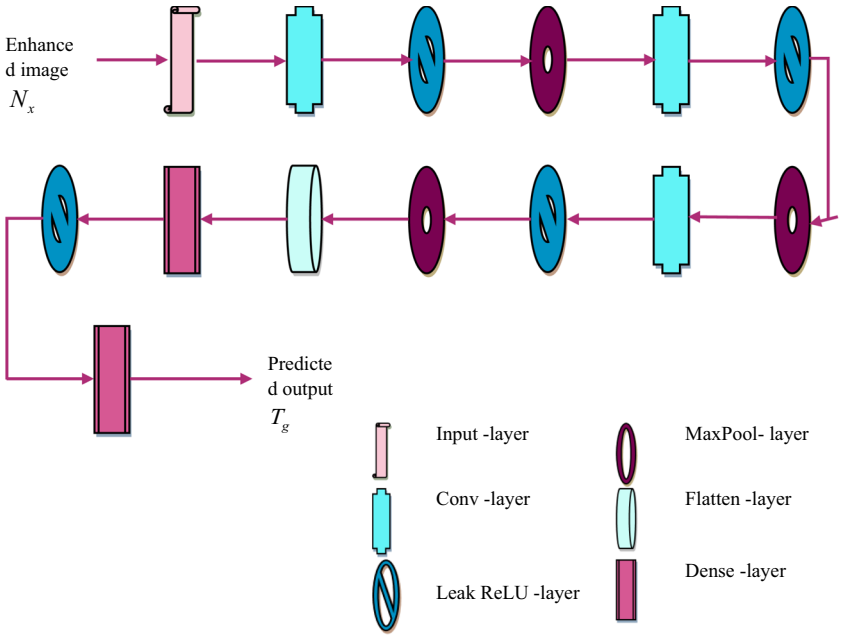


**Fig. 3** Architecture of DCNN

$$v_i^y = \partial(A_i^y) \quad with \sum_{\iota=1}^{\kappa_1^{\iota-1}} \sum_{\vartheta=\kappa_1^y}^{\kappa_1^y} \sum_{\omega=\kappa_2^y}^{\kappa_2^y} (\mathbb{Z}_{i,\iota}^y)_{\omega,\vartheta} * (A_{\mu}^{y-1})_{d+\vartheta,\chi+\omega} \tag{9}$$

Thus, the segmented image from DCNN is symbolized by $T_g$.The architecture of DCNN is displayed in Fig. 3.

**4.1.3.4 Multi-pooling SQA Network** Multi-Pooling-SQA network considers more segmentation quality cues than the first two networks. The Multi-Pooling-SQA network is built using two different types of quality cues: the segmented quality cue produced by applying multiple pooling operations and local context cue as utilized in ADD networks.

### 4.1.4 Training of CNN by Proposed FPCSO

FC [24] is a branch of applied mathematics that is essential for improving the performance of many algorithms. The FC is capable of solving integral and derivative equations. The algorithm's computing performance is improved by using the FC.

The main idea of POA [25] is to mimic natural hunting characteristics of pelicans. Pelicans serve as the searching agent in this optimization, looking for food sources. It is incredibly competitive and vastly valuable in handling optimization challenges. The POA demonstrated satisfactory performance in resolving design difficulties in real-time applications.CSA [26] is a population-based approach based on crow intelligence. It operates on the principle of hiding extra foods and retrieving them when needed. It achieved a higher convergence rate, and the solution to the researched issue was discovered fast. The three optimizations namely fractional concept, POA, and CSA have been combined as FPCSO for the purpose of improving images because of the advantages of each of the three optimizations.

**4.1.4.1 Pelican Solution Encoding** The MIRNet knowledge constraint $\mathfrak{O}$ in a exploration space $\mathbb{N}$ is proficient for locating best solution, which is exemplified as $\mathbb{N} = [1 \times \mathfrak{O}]$.

**4.1.4.2 Fitness Function** As indicated in the formula below, the fitness function is derived using the variances between the output of the SQA network and the desired output.

$$B = \frac{1}{\varphi} \sum_{g=1}^{\varphi} \left[T_g - L_g\right]^2 \tag{10}$$

wherein, total guidance images is oblique by $\varphi$, while target output is expressed as $L_g$, and SQA network output is signified as $T_g$.

FPCSO follows the methods outlined below to find the optimum answer.

#### 4.1.5 Step i: Initialization

Pelicans are regarded as population members, and these members are chosen at random to solve a problem. It can be modelled as follows:

$$\mathbb{Q} = \left\{\mathbb{Q}_1, \mathbb{Q}_2, ..., \mathbb{Q}_o, ..., \mathbb{Q}_p\right\} \tag{11}$$

wherein, $o$th candidate solution is indicated by $\mathbb{Q}_o$ while total count of variables in problem is represented by $p$, and the population is signified as $\mathbb{Q}$.

#### 4.1.6 Step ii: Evaluating Objective Function

Equation (10) is used to evaluate the goal function, with computation based on difference between MIRNet output and target output.

#### 4.1.7 Step iii: Moving Towards the Prey (Exploration)

Initially, pelicans locate prey and then migrate to the designated region. Pelican strategy modeling controls the scanning of the search space and the ability to

explore and construct a variety of search space areas. The random production of prey position in search space is referred to as a significant point in POA. As a result, the POA has increased exploration power in its precise search for problem-solving space. This is how it is expressed mathematically,

$$c_{sr}(\varpi + 1) = c_{sr}(\varpi) + rand\,(\tau_r - Y.c_{sr}(\varpi)) \tag{12}$$

$$c_{sr}(\varpi + 1) = c_{sr}(\varpi) + rand\,\tau_r - rand\,Y.c_{sr}(\varpi) \tag{13}$$

$$c_{sr}(\varpi + 1) = c_{sr}(\varpi)[1 - rand\,Y] + rand\,\tau_r \tag{14}$$

The updated equation of PCSO is exemplified by,

$$c_{sr}(\varpi + 1) = \frac{\partial_s \Delta_{sr}(\varpi) + \Im_r(\varpi)\,(rand\,Y - 1) + rand\,\tau_r(1 - \partial_s \Delta_{sr}(\varpi)}{(rand\;\; Y - \partial_s \Delta_{sr}(\varpi)} \tag{15}$$

Subtract $c_{sr}(\varpi)$ on both sides,

$$c_{sr}(\varpi + 1) - c_{sr}(\varpi) = \frac{\partial_s \Delta_{sr}(\varpi) + \Im_r(\varpi)\,(rand\,Y - 1) + rand\,\tau_r(1 - \partial_s \Delta_{sr}(\varpi)}{(rand\;\; Y - \partial_s \Delta_{sr}(\varpi)} - c_{sr}(\varpi) \tag{16}$$

The FC [24] is incorporated in this phase, the updated equation are obtained as,

$$J^q[c_{sr}(\varpi + 1)] = \frac{\partial_s \Delta_{sr}(\varpi) + \Im_r(\varpi)\,(rand\,Y - 1) + rand\,\tau_r(1 - \partial_s \Delta_{sr}(\varpi)}{(rand\;\; Y - \partial_s \Delta_{sr}(\varpi)} - c_{sr}(\varpi) \tag{17}$$

$$c_{sr}(\varpi + 1) - qc_{sr}(\varpi) - \frac{1}{2}qc_{sr}(\varpi + 1) - \frac{1}{6}(1 - q)c_{sr}(\varpi - 2) - \frac{1}{24}q\,(1 - q)\,(2 - q)\,c_{sr}(\varpi - 2) = \frac{\partial_s \Delta_{sr}(\varpi) + \Im_r(\varpi)\,(rand\,Y - 1) + rand\,\tau_r(1 - \partial_s \Delta_{sr}(\varpi)}{(rand\;\; Y - \partial_s \Delta_{sr}(\varpi)} - c_{sr}(\varpi) \tag{18}$$

$$c_{sr}(\varpi + 1) = (q - 1)\,c_{sr}(\varpi) + \frac{1}{2}q\,c_{sr}(\varpi - 1) + \frac{1}{6}(1 - q)\,c_{sr}(\varpi - 2) + \frac{1}{24}q\,(1 - q)(2 - q)c_{sr}(\varpi - 3) + \frac{\partial_s \Delta_{sr}(\varpi) + \Im_r(\varpi)(rand\,Y - 1) + rand\,\tau_r(1 - \partial_s \Delta_{sr}(\varpi))}{(rand\,Y - \partial_s \Delta_{sr}(\varpi))} \tag{19}$$

wherein, $\Im_r(\varpi)$ indicates memory of $r^{th}$ crow at $\varpi^{th}$ iteration, random number implies $\partial_1$, location of prey at $r^{th}$ dimension, $Y$ signifies parameter randomly equal to 1 or 2, random number between 0 and 1 symbolizes *rand*, flight length of crow represents $\Delta_{sr}(\varpi)$, $c_{sr}(\varpi)$ indicates location of pelican at $\varpi^{th}$ iteration, $c_{sr}(\varpi - 1)$ is location of the pelican at $(\varpi - 1)^{th}$ iteration, $c_{sr}(\varpi - 2)$ is location of the pelican at $(\varpi - 2)^{th}$ iteration, and $c_{sr}(\varpi - 3)$ is the location of the iteration $(\varpi - 3)^{th}$.

When optimization problem value is increased in that location, the newest site for pelicans is recognized. This type of update is defined to as efficient updating since algorithm avoids shifting to suboptimal locations. It is symbolized by,

$$F_\beta = \begin{cases} F_\beta(\tau+1), & \gamma_\beta(\tau+1) < \gamma_\beta \\ F_\beta, & else \end{cases} \tag{20}$$

wherein, $F_\beta(\tau+1)$ signifies $\beta$th pelican of fresher status, and $\gamma_\beta(\tau+1)$ represents value of impartial function founded upon this phase.

#### 4.1.8 Step iv: Winging Stage on Water Surface (Exploitation Phase)

When pelican reaches water's surface, it spreads its wings to propel a fish upward before catching its prey in its throat pouch. This strategy calls for pelicans to capture a large number of fish in the attacked area. Due to this behavior-based modeling of pelicans, POA in the hunting region converges to the best spots. In this process, POA gains greater local searching and exploitation capabilities. From a mathematical point of view, this method looks at nearby pelican positions to converge to the best answer. This pelican activity during a hunting season can be represented numerically as,

$$c_{sr}(\varpi_\infty+1) = c_{sr} + \mu\left(1-\frac{m}{X}\right)\cdot(2\,rand-1)\cdot c_{sr} \tag{21}$$

wherein, $\mu$ signifies constant that is equal to 1.2, $(\varpi_\infty+1)$ implies fresher status of $s$th pelican in $r$th dimension on basis of this step, $\mu\left(1-\frac{m}{X}\right)$ suggests locality radius of $c_{sr}$ while $m$ *and* $X$ signifies iteration amount and highest count of iteration. For local searches closer to each member in order to find the best answer, a coefficient "$\mu\left(1-\frac{m}{X}\right)$" is used. It works well at utilizing POA power to go closer to the ideal global answer. The region around each member is taken into consideration more in the beginning iterations since the coefficient value is larger. The coefficient decreases as replication is boosted by the algorithm, resulting in the smallest neighborhood radii for each individual member. As a result, the POA converges to a solution that is closer to the global optimum based on the usage idea by allowing for scanning the region around each individual member of the inhabitants with the smallest or most precise phases.

In this stage, a useful update is used to accept or reject a newer pelican position that can be created by,

$$F_\beta = \begin{cases} F_\beta(\tau_\infty+1), & \gamma_\beta(\tau_\infty+1) < \gamma_\beta \\ F_\beta, & else \end{cases} \tag{22}$$

wherein, $F_\beta(\tau_\infty+1)$ indicates fresher status of $\beta$th pelican and value of objective purpose based upon this step is implied by $\gamma_\beta(\tau_\infty+1)$.

#### 4.1.9 Step v: Termination

Once a better solution is found, the termination is carried out by continually completing FPCSO procedures. Algorithm 1 reveals the FPCSO pseudocode.

**Algorithm 1** Pseudocode of FPCSO

| SL. No | Algorithmic steps of FPCSO |
|---|---|
| Start POA | |
| 1 | **Input:** $c_{sr}(\varpi)$, $Y$ and $\mu$ |
| 2 | **Output:** $c_{sr}(\varpi+1)$ |
| 3 | **initiate** |
| 4 | Input in sequence of optimization trouble |
| 5 | Determine size of population and count of iterations $(X)$ |
| 6 | Adjust pelican position and compute objective function using equation (10) |
| 7 | ***For*** $m=1:X$ |
| 8 | Produce prey position arbitrarily |
| 9 | ***For*** $Y=1:L$ |
| 10 | Moving towards the prey phase |
| 11 | ***For*** $r=1:N$ |
| 12 | Evaluate fresher status of $r^{th}$ dimension using equation (15) |
| 13 | ***End*** |
| 14 | Update $s^{th}$ populace member using equation (20) |
| 15 | Winging on water surface phase |
| 16 | ***For*** $r=1:N$ |
| 17 | Evaluate fresher status of $s^{th}$ dimension using equation (21) |
| 18 | ***End*** |
| 19 | Apprise $r^{th}$ population adherent exploiting equation (22) |
| 20 | ***End*** |
| 21 | Apprise premium candidate solution |
| 22 | ***End*** |
| 23 | **Output:** Optimum candidate solution is achieved |
| 24 | ***End*** |
| 25 | **finish** |

For histopathology images of uterine tissue, the FPCSO algorithm effectively recognizes the segmentation with deep learning. The FPCSO algorithm successfully obtains global optima with the least amount of complexity by modifying the FC in relation to the PCSO approach.

## 5 Results and Discussion

This section describes study and discussion of FPCSO_enhanced SQA that was created in respect to assessment metrics using two datasets. Moreover, comparison studies are conducted to show the effectiveness of the suggested strategy.

### 5.1 Experimental Setup

FPCSO_enhanced SQA is run in the PYTHON tool on a computer with an Intel Core i3 processor and 4 GB of RAM.

### 5.2 Dataset Description

The database is built from [19], which consists of normal and pathological tissue photos of uterus endometrium that are then magnified and cropped as image samples. For the investigation, 400 image samples are acquired, 200 of which are normal and 200 of which are abnormal.

### 5.3 Experimental Outcomes

Figure 4 illustrates the results of the experiment that were obtained using FPCSO_enhanced SQA to improve the appearance of uterine tissue histopathology pictures. Figure 4a–c show the input picture-20, the filtered image-20, and the segmented

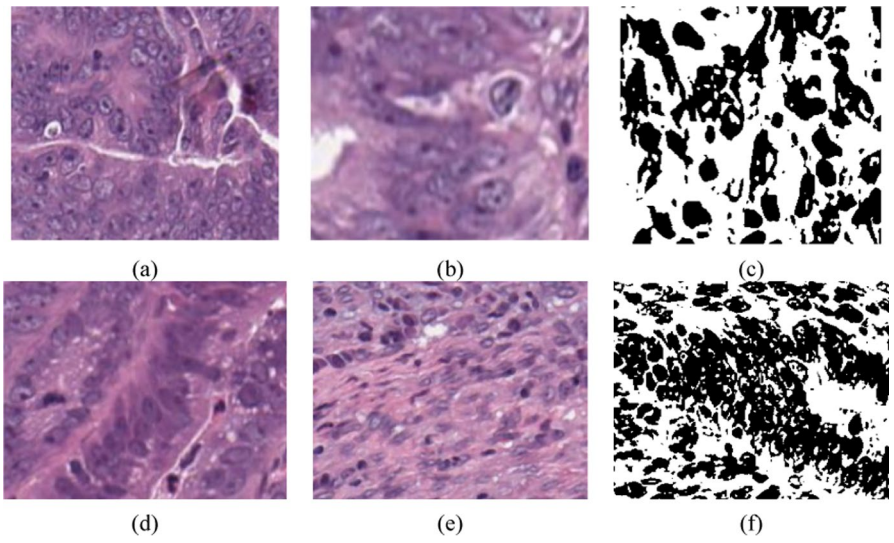


**Fig. 4** Experimental outcome, **a** Input image-20, **b** filtered image-20, and **c** segmented image-20, **d** input image-40, **e** filtered image-40, and **f** segmented image-40

image -20, whereas Fig. 4d–f provide the input image-40, the filtered image-40, and the segmented image -40.

### 5.4 Evaluation Measures

Evaluation measures, PSNR, MSE, and DD, which are outlined in the following subsections, are used to assess FPCSO_enhanced SQA.

#### 5.4.1 PSNR

PSNR is described as ratio of maximum practical power of a picture to power of corrupting noises, which influences quality of portrayal. It is expressed in decibels (dB) and is model able using,

$$\varsigma = 10 \log_{10} \left( \frac{\mathbb{R}^2}{\varepsilon} \right) \tag{23}$$

Here,$\mathbb{R}$ indicates highest possible power of an image and $\varepsilon$ designates MSE.

#### 5.4.2 MSE

A cumulative squared error between the improved and original images is what is referred to as an MSE and is determined using the equation below.

$$\varepsilon = \frac{1}{j} \sum_{n=1}^{j} [W_n - M_n]^2 \tag{24}$$

Here,$j$ signifies overall image samples, $W_n$ and $M_n$ are enhanced image and original image.

#### 5.4.3 DD

DD denotes the degree to which an image is distorted, and it may be calculated using the equation below.

$$\delta (M^*, M) = \frac{1}{SN} \parallel vec (M^*) - vec (M) \parallel \tag{25}$$

Here, matrix vectors of $M^*$ and $M$ are designated by $vec (M^*)$ $and$ $vec$ $(M)$.

### 5.5 Comparative Techniques

To demonstrate the efficacy of the created FPCSO_enhanced SQA, it is compared to other studied techniques such as fusion based classifier [10], SLN [15], Morphological + thresholding [9], markers of immunogenicity [16] and PCSO_MIRNet [17].

### 5.6 Comparative Assessment

The strategies discussed above are evaluated with FPCSO_enhanced SQA while taking evaluation measures into account by adjusting training data.

#### 5.6.1 Analysis Based on Training Data

When the percentage of training data is increased from 50 to 90%, Fig. 5 shows how the assessment of comparison with FPCSO enhanced SQA is interpreted. Fig. 5a depicts the analysis of FPCSO enhanced SQA in terms of PSNR. PSNR obtained by FPCSO_enhanced SQA is 49.574 dB, whereas fusion-based classifier, SLN, Morphological + thresholding, markers of immunogenicity and PCSO_MIRNet attained values of 44.833 dB, 44.206, 45.246 dB, 48.089 dB, and 48.222 dB for data percentage of 90%.Fig. 5b depicts a comparison of FPCSO_enhanced SQA to MSE. When the data percentage is 90%, the MSE obtained by FPCSO_enhanced SQA is 0.975, whereas the MSE obtained by fusion-based classifier, SLN, Morphological + thresholding, markers of immunogenicity, and PCSO_MIRNet were 2.019,

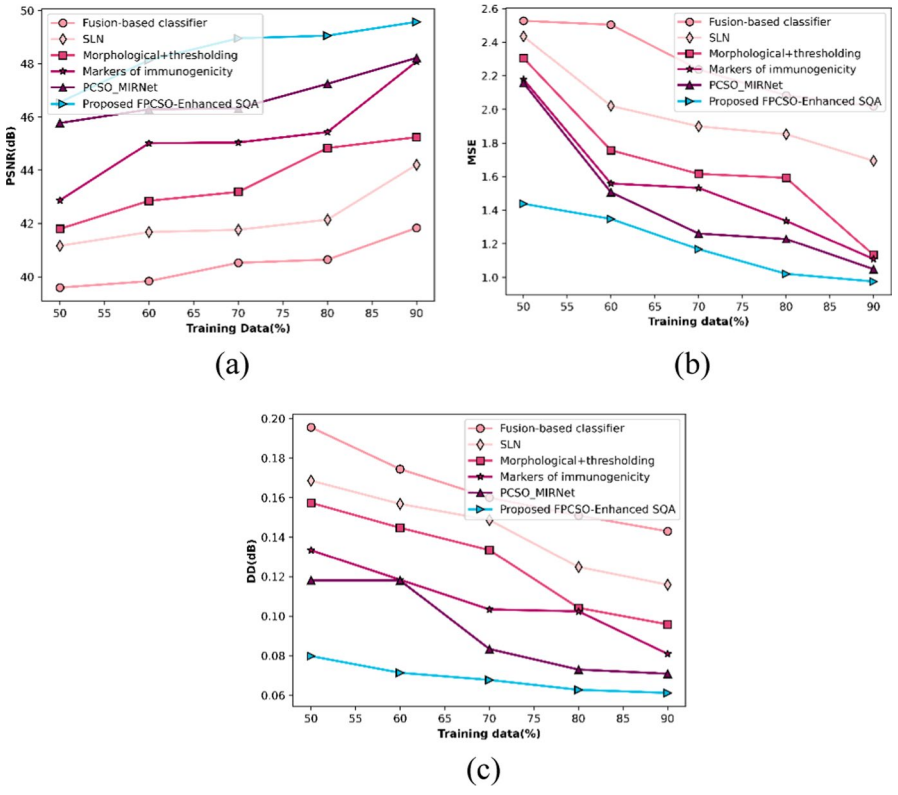


**Fig. 5** Comparative assessment of FPSCO_enhanced SQA based on **a** PSNR, **b** MSE, and **c** DD

1.694, 1.133, 1.109, and 1.049.Fig. 5c provides more details on the calculation of FPCSO_enhanced SQA based on DD. DD achieved by FPCSO_enhanced SQA is 0.061 dB, compared to fusion-based classifier is 0143 dB, SLN is 0.116 dB, Morphological + thresholding is 0.096 dB, markers of immunogenicity is 0.081 dB, and PCSO_MIRNet is 0.071 dB, with 90% of the data percentage.

### 5.7 Performance Assessment

By varying the amount of training data with different epochs, Fig. 6 shows how performance for the FPCSO-enhanced SQA is assessed. Figure 6a depicts an evaluation of performance based on PSNR. When 90% of the data is present, the PSNR obtained by FPCSO enhanced SQA with epoch 10 is 39.893 dB, followed by values of 42.922 dB, 44.581 dB, 45.737 dB, and 47.957 dB. Figure 6b explains how to estimate performance in terms of MSE. With training percentage of 90%, performance assessment for FPCSO enhanced SQA regarding MSE with epochs 10, 20, 30, 40, and 50 is 2.122 dB, 1.910 dB, 1.544 dB, 1.366 dB, and 1.137 dB. The assessment of performance in relation to DD is explained in Fig. 6c.When percentage of data is

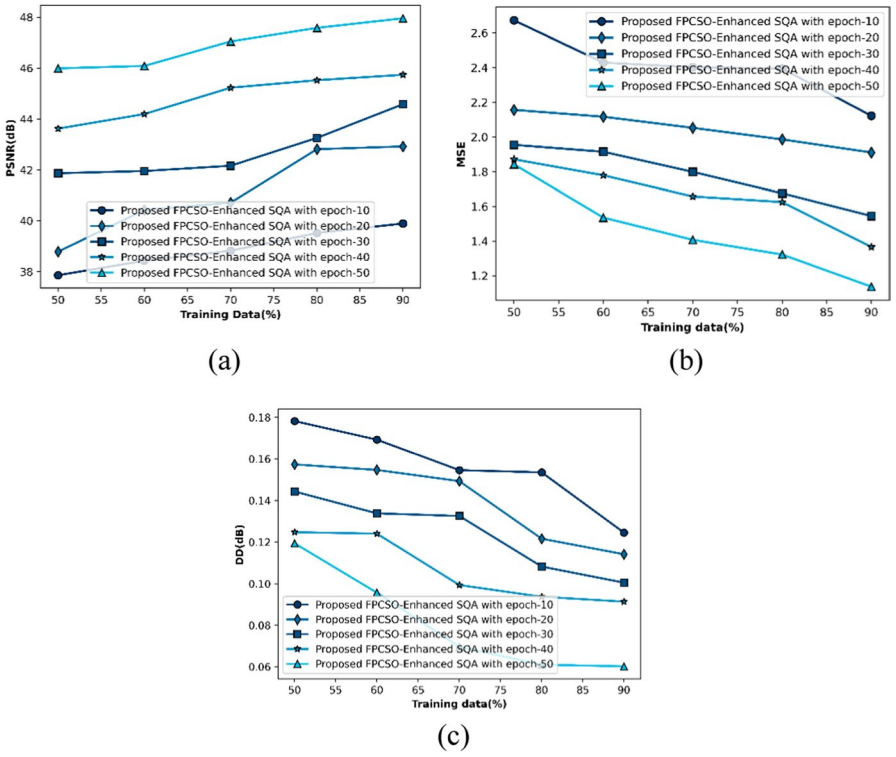


**Fig. 6** Performance evaluation of FPCSO_enhanced SQA, with respect to **a** PSNR, **b** MSE, and **c** DD

90%, DD obtained by FPCSO_enhanced SQA with epochs 10, 20, 30, 40 and 50 are 0.125 dB, 0.114 dB, 0.100 dB, 0.091 dB and 0.060 dB.

### 5.8 Algorithmic Methods

For determining the effectiveness of the created method, the FPCSO + enhanced SQA algorithm is compared to several existing algorithms such as anti-corona virus optimization (ACVO) [27] + enhanced SQA, Political Optimizer (PO) [28] + enhanced SQA, CSA [26] + enhanced SQA, and POA [25] + enhanced SQA. It is estimated using assessment measures and varied iterations from 10 to 50.

### 5.9 Algorithmic Evaluation

Figure 7 depicts an algorithmic estimation of the FPCSO + enhanced SQA method in terms of performance measures by different iterations.Fig. 7a depicts the assessment of PSNR. When iteration is set to 50%, the PSNR obtained by the FPCSO + enhanced SQA algorithm is 49.574 dB, while the PSNR obtained by the ACVO + enhanced SQA, PO + enhanced SQA, CSA + enhanced SQA,

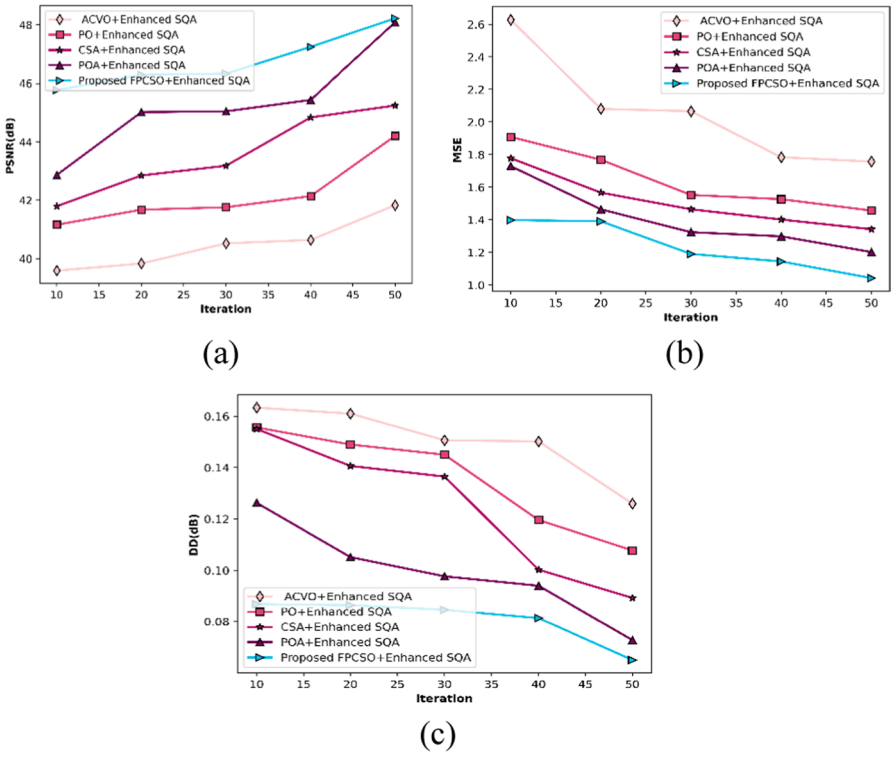


**Fig. 7** Algorithmic consideration based on **a** PSNR, **b** MSE, and c DD

and POA + enhanced SQA algorithms are 41.833 dB, 44.206 dB, 45.246 dB, and 48.222 dB.Fig. 7 b) depicts the MSE evaluation. When iteration is 50%, the MSE obtained by the FPCSO + enhanced SQA method is 1.043, whereas current techniques such as ACVO + enhanced SQA, PO + enhanced SQA, CSA + enhanced SQA, and POA + enhanced SQA obtained 1.758, 1.457, 1.343, and 1.203.Fig. 7c depicts the DD analysis. While iteration is 50%, the DD achieved by FPCSO + enhanced SQA is 0.065 dB, but ACVO + enhanced SQA is 0.126 dB, PO + enhanced SQA is 0.108 dB, CSA + enhanced SQA is 0.089B, and POA + enhanced SQA is 0.073 dB. As a result, the FPCSO + enhanced SQA algorithm outperforms traditional methods.

#### 5.9.1 Comparative Discussion

This comparative discussion shows that the proposed FPCSO_enhanced SQA method is compared with various techniques such as fusion based-classifier, SLN, Morphological + thresholding, markers of immunogenicity, and PCSO_MIRNet for histopathological images of uterine tissue. It shows that the proposed technique has minimum MSE, high PSNR, and very low DD.

#### 5.9.2 Technique Evaluation

Table 1 compares FPCSO_enhanced SQA to some reviewed methodologies and shows the best results. As a result, FPCSO_enhanced SQA acquired a maximum PSNR value of 49.574 dB and a minimum MSE and DD value of 0.975 and 0.061 dB for training data, respectively.

#### 5.9.3 Algorithm Analysis

This algorithmic discussion compares the proposed FPCSO_enhanced SQA approach to other techniques for histopathology imaging of uterine tissue, including ACVO + enhanced SQA, PO + enhanced SQA, CSA + enhanced SQA, and POA + enhanced SQA. It demonstrates that the proposed approach has a low MSE, a high PSNR, and a very low DD. Table 2 compares FPCSO enhanced SQA to some of the approaches evaluated and displays the best results. As a result, using training data, FPCSO_enhanced SQA achieved a greatest PSNR value of 49.574 dB and a least MSE and DD value of 1.042 and 0.065 dB, correspondingly.

## 6 Conclusion

Endometrial cancer, also known as uterine cancer, has a serious impact on female reproductive systems, and the assessment of a histological image is gold standard for diagnose endometrial cancer. Additionally, the classification of diseases and healthy uterine tissues is thought to benefit greatly from the enhancement of histopathological pictures. Moreover, pathologists could not understandably confirm the results of their diagnoses using the procedures that were already available. In order to develop appearance of histopathological images of uterine tissue, a method known

**Table 1** Comparative discussion of FPCSO_enhanced SQA

| Analysis based on | Metrics/methods | Fusion based-classifier | SLN | Morphological + thresholding | Markers of immunogenicity | PCSO_MIRNet | Proposed FPCSO_ enhanced SQA |
|---|---|---|---|---|---|---|---|
| Training data = 90% | *PSNR (dB)* | 41.833 | 44.206 | 45.246 | 48.089 | 48.222 | **49.574** |
| | *MSE* | 2.019 | 1.694 | 0.133 | 1.109 | 1.049 | **0.975** |
| | *DD (dB)* | 0.143 | 0.116 | 0.096 | 0.081 | 0.071 | **0.061** |

Bold values indicate the best performance

**Table 2** Algorithmic discussion of FPCSO_enhanced SQA

| Analysis based on | Metrics/Methods | ACVO + enhanced SQA | PO + enhanced SQA | CSA + enhanced SQA | POA + enhanced SQA | Proposed FPCSO_ enhanced SQA |
|---|---|---|---|---|---|---|
| Iteration 50% | *PSNR (dB)* | 41.833 | 44.206 | 45.246 | 48.089 | **49.574** |
| | *MSE* | 1.757 | 1.457 | 1.342 | 1.202 | **1.042** |
| | *DD(dB)* | 0.125 | 0.107 | 0.089 | 0.727 | **0.065** |

Bold values indicate the best performance

as FPCSO_enhanced SQA is introduced. When a database is first constructed, 400 image samples are acquired, of which 200 are normal and 200 are aberrant. The image is then pre-processed using a median filter, which improves image excellence and removes noise from the image. Following that, image enhancement is carried out using MIRNet, which is done using PCSO. Furthermore, the tissue segmentation is done by using proposed segmentation quality assessment network, where parameters election is based on DCNN, which is trained by using proposed FPCSO. Moreover, the introduced FPCSO is a novel method created by the integration of FC, PSO, and CSA. The FPCSO_enhanced SQA obtained maximum PSNR of 49.574 dB, least MSE of 0.975 and least DD of 0.061 dB. The developed method is used in a wide range of clinical applications, including medical diagnosis, successful prediction treatment, and cancer grading. The main limitation of this research is failed to include more performance metrics for comparative assessment. The future work will be performed using different datasets for the implementation of the histopathological images of uterine tissue.

**Acknowledgements** I would like to express my very great appreciation to the co-authors of this manuscript for their valuable and constructive suggestions during the planning and development of this research work.

**Author contribution** All authors have made substantial contributions to conception and design, revising the manuscript, and the final approval of the version to be published. Also, all authors agreed to be accountable for all aspects of the work in ensuring that questions related to the accuracy or integrity of any part of the work are appropriately investigated and resolved.

**Funding** This research did not receive any specific funding.

**Data availability** The data underlying this article are available in Cancer imaging archive dataset, at https://www.cancerimagingarchive.net/datascope/cptac/home/.

## Declarations

**Conflict of interest** The authors declare no conflict of interest.

**Ethical approval** Not Applicable.

**Informed consent** Not Applicable.

## References

1. Ayyad, S. M., Shehata, M., Shalaby, A., Abou El-Ghar, M., Ghazal, M., El-Melegy, M., Abdel-Hamid, N. B., Labib, L. M., Ali, H. A., & El-Baz, A. (2021). Role of AI and histopathological images in detecting prostate cancer: A survey. *Sensors, 21*(8), 2586.
2. Kumar, M. D., Babaie, M., Zhu, S., Kalra, S. and Tizhoosh, H. R. (2017), A comparative study of CNN, BoVW and LBP for classification of histopathological images, In 2017 IEEE Symposium Series on Computational Intelligence (SSCI), pp. 1–7, IEEE.
3. Yurttakal, A. H. and Erbay, H. (2020) Segmentation of larynx histopathology images via convolutional neural networks", Intelligent and Fuzzy Techniques: Smart and Innovative Solutions.

4. Yurttakal, H. A., Erbay, H., Çinarer, G., & Baş, H. (2021). Classification of diabetic rat histopathology images using convolutional neural networks. *International Journal of Computational Intelligence Systems, 14*(1), 715–722.
5. Gurcan, M. N., Boucheron, L. E., Can, A., Madabhushi, A., Rajpoot, N. M., & Yener, B. (2009). Histopathological image analysis: A review. *IEEE Reviews in Biomedical Engineering, 2*, 147–171.
6. Filipczuk, P., Fevens, T., Krzyżak, A., & Monczak, R. (2013). Computer-aided breast cancer diagnosis based on the analysis of cytological images of fine needle biopsies. *IEEE Transactions on Medical Imaging, 32*(12), 2169–2178.
7. Kang, Q., Lao, Q. and Fevens, T. (2019), Nuclei segmentation in histopathological images using two-stage learning", In Medical Image Computing and Computer Assisted Intervention–MICCAI 2019: 22nd International Conference, Shenzhen, China, Proceedings, Part I,vol. 22, pp. 703–711, Springer International Publishing.
8. Guo, P., Banerjee, K., Stanley, R. J., Long, R., Antani, S., Thoma, G., Zuna, R., Frazier, S. R., Moss, R. H., & Stoecker, W. V. (2015). Nuclei-based features for uterine cervical cancer histology image analysis with fusion-based classification. *IEEE Journal of Biomedical and Health Informatics, 20*(6), 1595–1607.
9. Patil, S. R. and Patil, V. I. (2020), Detection of nuclei cell in histopathological images of uterine cancer: Adenocarcinoma of endometrium", In 2020 4th International Conference on Trends in Electronics and Informatics (ICOEI), vol. 48184, pp. 888–893, IEEE.
10. Qu, X. M., Velker, V. M., Leung, E., Kwon, J. S., Elshaikh, M. A., Kong, I., Logie, N. A., Mendez, L. C., van der Putten, L. J., Donovan, E. K., & Munkarah, A. R. (2018). The role of adjuvant therapy in stage IA serous and clear cell uterine cancer: A multi-institutional pooled analysis. *Gynecologic oncology, 149*(2), 283–290.
11. Neofytou, M. S., Tanos, V., Constantinou, I., Kyriacou, E. C., Pattichis, M. S., & Pattichis, C. S. (2014). Computer-aided diagnosis in hysteroscopic imaging. *IEEE Journal of Biomedical and Health Informatics, 19*(3), 1129–1136.
12. Konrad, J., Merck, D., Wu, J. Y., Tuomi, A., & Beland, M. (2018). Improving ultrasound detection of uterine adenomyosis through computational texture analysis. *Ultrasound Quarterly, 34*(1), 29–31.
13. Sun, H., Zeng, X., Xu, T., Peng, G., & Ma, Y. (2019). Computer-aided diagnosis in histopathological images of the endometrium using a convolutional neural network and attention mechanisms. *IEEE journal of biomedical and health informatics, 24*(6), 1664–1676.
14. Song, Y. and Liu, J., "An improved adaptive weighted median filter algorithm", In Journal of Physics: Conference Series, vol. 1187, no. 4, pp. 042107, IOP Publishing, April, 2019.
15. Wright, J. D., Cham, S., Chen, L., Burke, W. M., Hou, J. Y., Tergas, A. I., Desai, V., Hu, J. C., Ananth, C. V., Neugut, A. I., & Hershman, D. L. (2017). Utilization of sentinel lymph node biopsy for uterine cancer. *American journal of obstetrics and gynecology, 216*(6), 594-e1.
16. Jones, N. L., Xiu, J., Rocconi, R. P., Herzog, T. J., & Winer, I. S. (2020). Immune checkpoint expression, microsatellite instability, and mutational burden: Identifying immune biomarker phenotypes in uterine cancer. *Gynecologic Oncology, 156*(2), 393–399.
17. Alshdaifat, E. H., El-Deen Al-Horani, S. S., Al-Sous, M. M., Al-Horani, A. S., Sahawneh, F. E. and Sindiani, A. M. (2022) Histopathological pattern of endometrial biopsies in patients with abnormal uterine bleeding in a tertiary referral hospital in Jordan", Annals of Saudi Medicine, *42*(3), 204-213.
18. Solar, M. and Gonzalez, J.P.P. (2019), "Computational detection of cervical uterine cancer", In 2019 Sixth International Conference on eDemocracy& eGovernment (ICEDEG), pp. 213–217, IEEE, April, 2019.
19. Cancer imaging archive dataset is taken from, "https://www.cancerimagingarchive.net/datascope/cptac/home/", accessed on February, 2022.
20. Deshmukh, M. (2021) Underwater image enhancement using improved bat algorithm, Multimedia Research, *4*(2).
21. Zamir, S. W., Arora, A., Khan, S., Hayat, M., Khan, F. S., Yang, M. H. and Shao, L., "Learning enriched features for real image restoration and enhancement, In Computer Vision–ECCV 2020: 16th European Conference, Glasgow, UK, August 23–28, 2020, Proceedings, Part XXV vol. 16, pp. 492–511, Springer International Publishing, 2020.
22. Meng, F., Guo, L., Wu, Q., & Li, H. (2019). A new deep segmentation quality assessment network for refining bounding box-based segmentation. *IEEE Access, 7*, 59514–59523.

23. Tu, F., Yin, S., Ouyang, P., Tang, S., Liu, L., & Wei, S. (2017). Deep convolutional neural network architecture with reconfigurable computation patterns. *IEEE Transactions on Very Large-Scale Integration (VLSI) Systems, 25*(8), 2220–2233.
24. Bhaladhare, P.R. and Jinwala, D.C. (2014) A clustering approach for the l-diversity model in privacy preserving data mining using fractional calculus-bacterial foraging optimization algorithm", Advances in Computer Engineering.
25. Trojovský, P., & Dehghani, M. (2022). Pelican optimization algorithm: A novel nature-inspired algorithm for engineering applications. *Sensors, 22*(3), 855.
26. Askarzadeh, A. (2016). A novel metaheuristic method for solving constrained engineering optimization problems: Crow search algorithm. *Computers & structures, 169*, 1–12.
27. Emami, H. (2022). Anti-coronavirus optimization algorithm. *Soft Computing, 26*(11), 4991–5023.
28. Askari, Q., Younas, I., & Saeed, M. (2020). Political optimizer: A novel socio-inspired meta-heuristic for global optimization. *Knowledge-Based Systems, 195*, 105709.



## Authors and Affiliations

### Veena I. Patil[1,2] · Shobha R. Patil[3]

✉ Veena I. Patil
vapatil@bldeacet.ac.in

[1] Department of Computer Science and Engineering, Basaveshwar Engineering College, Bagalkote, Karnataka 587102, India

[2] BLDEA's V. P Dr P. G Halakatti College of Engineering and Technology, Vijayapura, Karnataka 586103, India

[3] Information Science and Engineering, Department of Information Science and Engineering, Basaveshwar Engineering College/ Visvesveraya Technological University, Bagalkote, Karnataka 587102, India